Proceedings of the ASME 2018 International Technical Conference and Exhibition on Packaging and Integration of Electronic and Photonic Microsystems
InterPACK2018
August 28-30, 2018, San Francisco, CA, USA

IPACK2018-8468

PRACTICAL CONCERNS FOR ADOPTION OF MICROJET COOLING

Stephen M. Walsh
MIT Lincoln Laboratory
Lexington, MA, USA

James P. Smith
MIT Lincoln Laboratory
Lexington, MA, USA

Eric A. Browne
MIT Lincoln Laboratory
Lexington, MA, USA

Timothy W. Hennighausen
MIT Lincoln Laboratory
Lexington, MA, USA

Bernard A. Malouin
MIT Lincoln Laboratory
Lexington, MA, USA

ABSTRACT

As power densities in advanced electronics continue to rise, the need for high performance thermal solutions becomes increasingly important. Liquid jet impingement has been applied to cooling high power-density electronics due to its ability to dissipate large heat fluxes while maintaining an acceptable operating temperature in the device. Recently, microjets have been embedded within the device substrate, forming a compact solution that is highly scalable. Many practical questions remain, however, on whether microjet technology is ready for actual implementation. In this work, we address several important questions that impede adoption of the technology. Numerical analysis and experimental data are provided to demonstrate the tradeoff between thermal performance and driving pressure requirements through pumping analysis. Additional mechanical concerns regarding robustness to clogging and resistance to erosion are addressed through a 1000-hour extended lifetime test.

INTRODUCTION

The scaling down of electronic device dimensions, and the corresponding increase in power density, has necessitated the development of new cooling methods. Current cooling technologies have shifted away from expensive and large size, weight and power (SWaP) cooling approaches, in favor of liquid cooling embedded at the substrate level.

Jet impingement has been used for several decades for high heat flux applications such as turbine cooling and quenching metals, and it has recently been applied for cooling high power density electronic components [1-3]. In jet impingement, a stream of fluid interacts with a solid surface producing high convective heat transfer coefficients, particularly in the impingement zone at the jet centerline. Similar to trends seen with other thermal management approaches, including microchannels, heat transfer effectiveness improves as jet diameters are scaled down to less than one millimeter, forming microjets [4-5]. Unlike microchannels, however, microjet impingement offers several advantages including generally higher heat transfer coefficients, lower pressure drops, and less significant temperature gradients when the jets are used in arrays [6].

Like other cooling technologies, microjets can be evaluated by their ability to dissipate heat energy per unit area and per unit temperature rise, quantified with the heat transfer coefficient, h,

$$h = \frac{q}{A(T_s - T_f)} \quad (1)$$

where q is the power dissipated in the device, A is the cooled area, T_s is the local surface temperature, and T_f is the local fluid temperature at the point of interaction. Previous researchers have demonstrated strong heat transfer performance (i.e., very high heat transfer coefficients) using arrays of single-phase microjets. Fabbri and Dhir achieved heat transfer coefficients of 60,000 W/m^2K with diameters 69 µm to 250 µm [7]. Overholt et al. used jet diameters of 300 and 635 µm to achieve heat transfer coefficients of 280,000 W/m^2K [8]. Browne et al. and Michna et al. obtained heat transfer coefficients of 414,000 W/m^2K with 112 µm diameter jets [9-10].

The extent to which these high heat transfer coefficients are achieved depends on both geometrical features (including jet

This material is based upon work supported by the Assistant Secretary of Defense for Research and Engineering under Air Force Contract No. FA8721-05-C-0002 and/or FA8702-15-D-0001. Any opinions, findings, conclusions or recommendations expressed in this material are those of the author(s) and do not necessarily reflect the views of the Assistant Secretary of Defense for Research and Engineering.

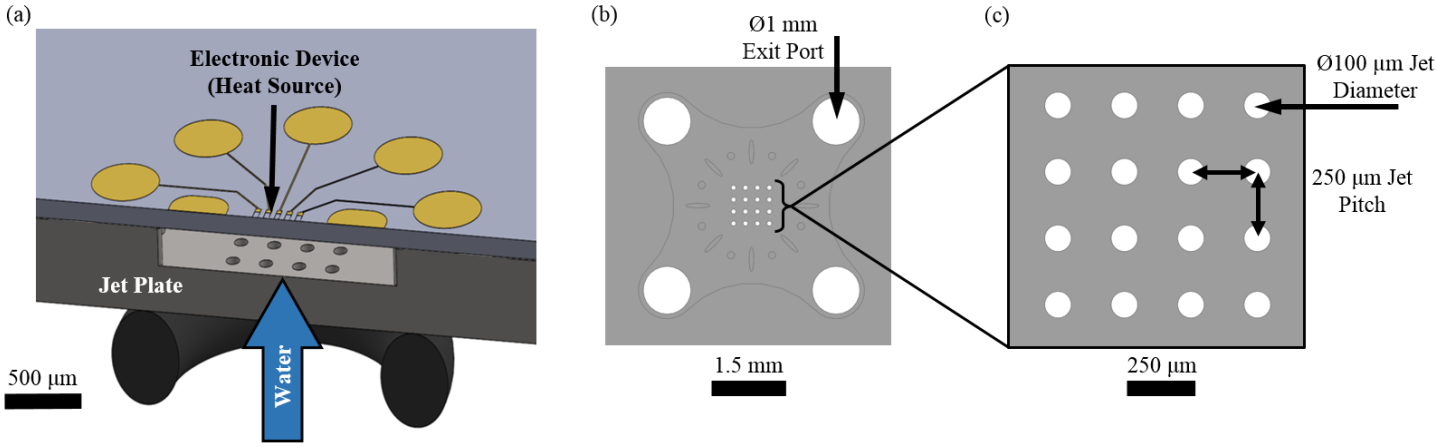

Figure 1: (a) Assembly of the integrated heater and microjet array with water jet impingement from the bottom. (b) Full view of the microjet plate with the array of 16 jets at the center of the clover shaped well. (c) Array geometry of 100 µm diameter orifices with 250 µm spacing.

diameter, jet-to-jet spacing and jet-to-target distance) and flow properties (such as fluid thermal properties and flow rate). Two important parameters for understanding the effect of flow rate on heat transfer are the Reynolds and Nusselt numbers defined as

$$Re_d = \frac{\rho V_{jet} D}{\mu} \quad (2)$$

$$Nu_d = \frac{hD}{k} \quad (3)$$

where the Reynolds number is a ratio of inertial forces to viscous forces and the Nusselt number is a dimensionless heat transfer performance term. Michna et al. [10] performed a study investigating the effect of area ratio (A_r), defined as the total area of the jets divided by the cooled surface area, and flow rate on submerged and confined microjets with the following non-dimensional correlation

$$Nu_d = 0.675 Re_d^{0.55} Pr^{0.243} \cos(5.416 A_r - 1.259) \quad (4)$$

where the heat transfer performance depends on the dimensionless velocity (Re_d), fluid thermal properties (Pr), and the area ratio of the microjet geometry [10]. As seen in Equation 4, heat transfer performance scales with velocity raised to the exponent of 0.55. This relationship shows that doubling the jet velocity results in a 1.5x increase in heat transfer performance. The pressure drop across the device scales with velocity squared, so although higher performance can be achieved with increasing velocity, it requires higher driving pressure. Here, we further investigate this through fully coupled numerical analysis to illustrate the tradeoffs between thermal performance and driving pressure requirements.

An additional concern that must be considered when implementing jet impingement for electronics cooling is susceptibility to clogging. Clogging occurs when particles are introduced to the flow loop (from outside, or generated within the loop) impeding flow through one of the 100 µm diameter jets. A consequence of clogging would be a sudden increase in the required driving pressure of the system, due to the corresponding decrease in microjet cross sectional area. Alternatively, with a fixed driving pressure, the flow rate through the microjets would decrease. More importantly, in both cases, clogging can adversely affect the array's ability to provide uniform cooling. Here, we provide experimental evidence of extended, clog-free operation of microjets using only commercially available, low-cost filters.

Finally, erosion of the backside of the electronic device is also a potential concern for jet impingement as a long term solution. Ditri et al. [11] used a computational approach (Lagrangian Particle Tracking) to explore the effects of erosion for a distribution of particle sizes ranging from 0.5 to 5.4 µm on the back of a 4 µm thick Au gold coating. Their numerical study showed that small particles (0.5 µm diameter) followed the fluid streamlines whereas larger particles (5+ µm diameter) experienced impact with the wall due to their larger inertial forces. They used these results to predict the lifetime of the 4 µm Au coating and to select a filter to block out larger particles. In this study, we complement the previous numerical work with experimental results for extended erosion testing with maximum particle sizes of 10 µm under normal working conditions.

EXPERIMENTAL METHODS

In this work, an embedded microjet architecture was designed and fabricated shown in Fig. 1a. Water is used as the working fluid, entering vertically through the microjet orifices to impinge on the backside of the electronic device. The electronic device is a titanium nitride (TiN) resistive heater, which generates heat due to Joule heating effects. The TiN ceramic heater was deposited on a 200 µm thick silicon substrate. Bonded to this heater was a second silicon layer with the microjet array. The microjet geometry was etched into this 450 µm silicon wafer. Both the integrated heater and jet wafer were diced to 20 mm x 20 mm and bonded together.

The design methodology and fabrication details of the microjet array geometry are presented in Ref. [3]. This particular microjet array, shown in the center of Fig. 1b, consists of a 4 x 4 array at the center of a 200 µm deep, clover shaped well. At the four corners of the well are exit ports, each 1 mm in diameter to

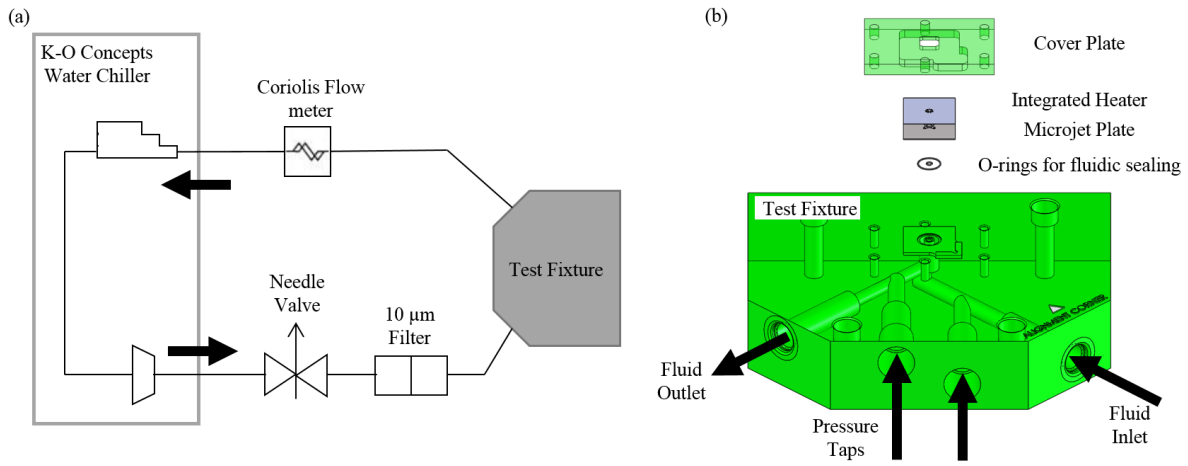

Figure 2: (a) Closed flow loop used to provide water to the microjet array. (b) Translucent, exploded view of the test fixture used to hold the microjet cooled assembly in place.

minimize pressure losses. The 16 microjets were 100 µm diameter with 250 µm pitch jet-to-jet. Additionally, a ring of support features surrounds the microjet array.

A closed flow loop shown in Fig. 2a was constructed to examine the performance of the microjet cooling. The flow loop supplied the microjet orifices with water at a controllable flow rate while measuring the upstream pressure, downstream pressure, and the flow rate. The flow loop consisted of a recirculating water chiller (LCR-8-G2, K-O Concepts) connected with stainless steel braided tubing (3/8", Swagelok). The recirculating chiller delivered fluid to the microjets at a 20 °C set point and up to 70 psi. The flow rate was measured by a Coriolis flow meter (Micro Motion CMFS025M, Emerson). Fine flow rate control was achieved with a needle valve (SS-1RS6, Swagelok). A 10 µm sintered metal filter (SS-6TF-10, Swagelok) filtered out particles larger than 10 µm in size.

To hold the microjet assembly in place, a test fixture made of polyether ether ketone (PEEK) was designed and built. PEEK was chosen because it is dimensionally stable, easy to machine, has a low thermal conductivity (k = 0.25 W/m-K) and high melting point (T_{mp} = 343 °C). An inlet fluid channel supplied water to the microjets through a vertical inner annulus and then the exit flow was captured by an outer annulus connected to a fluid outlet channel. Pressure transducers (PX329-111A5V, Omega) were placed in pressure taps of the fluid inlet and outlet channels providing fluid pressure measurements before and after the device under test. A cover plate provided compressive force, which sealed O-rings for the inner and outer cylinders.

One of the key challenges during experimentation was selection of a flow meter with high accuracy at low flow rates. As will be discussed in this paper, microjets achieve high performance at relatively low flow rates (100-200 mL/min). The Coriolis meter is capable of measuring flow rates down to 50 mL/min with 0.1% accuracy. An additional challenge was selecting suitable O-rings for fluidic sealing at such small scale. The O-rings needed to be sized correctly to seal the fluid, without blocking any of the jet orifices. The inner annulus O-ring, which sealed the fluid inlet before the microjet orifices, was 1.75 mm in diameter and the outer O-ring, which sealed the fluid outlet, was 8 mm in diameter. Alignment had to be carefully completed to avoid the O-ring obstructing the corner microjets in the array.

RESULTS AND DISCUSSION

Thermal Performance Tradeoffs

The local heat transfer coefficient, defined in Eq. 1, depends on surface and fluid temperatures at the point of interaction, which are difficult to measure experimentally. To this end, a numerical model was constructed to predict the ability of the microjets to cool the integrated heater, specifically at varying flow rates. This was done by calculating the convective heat transfer coefficient due to the energy exchange between the fluid and the heated surface. A fully conjugate computational fluid dynamics (CFD) and heat transfer model was developed in COMSOL Multiphysics 5.2a. Details of the numerical model can be found in [3], including comparison of the model to experiment. The computational model is also a powerful tool for visualizing the complex fluid dynamics occurring in the assembly. Figs. 3a- 3c show the magnitude of the fluid velocity on a color map at three different inlet jet velocities of 10, 15, and 20 m/s, with a zero pressure boundary condition on the exit ports.

The fluid dynamic analysis in Figs. 3a-3c showed that the jets entered the cavity at a uniform velocity. After entering the cavity, the microjets entrained local fluid as they proceeded toward the wall. At the center of the entering flow, the potential core develops, which remains at the entrance velocity. At the impingement surface near the jet centerline, the fluid velocity was close to zero. This indicated the high pressure region, known as the stagnation zone, where the greatest amount of heat transfer occurs. The heat transfer is highest here due to the suppression of the thermal boundary layer caused by the microjet's momentum. Radially away from the stagnation zone, the flow is directed parallel to the surface in the wall jet. Additional regions of low fluid velocity occur where wall jets of adjacent jets interact in what are known as secondary stagnation points. These do not produce high heat transfer coefficient regions. The stagnation point and secondary stagnation point are identified in Fig. 3c.

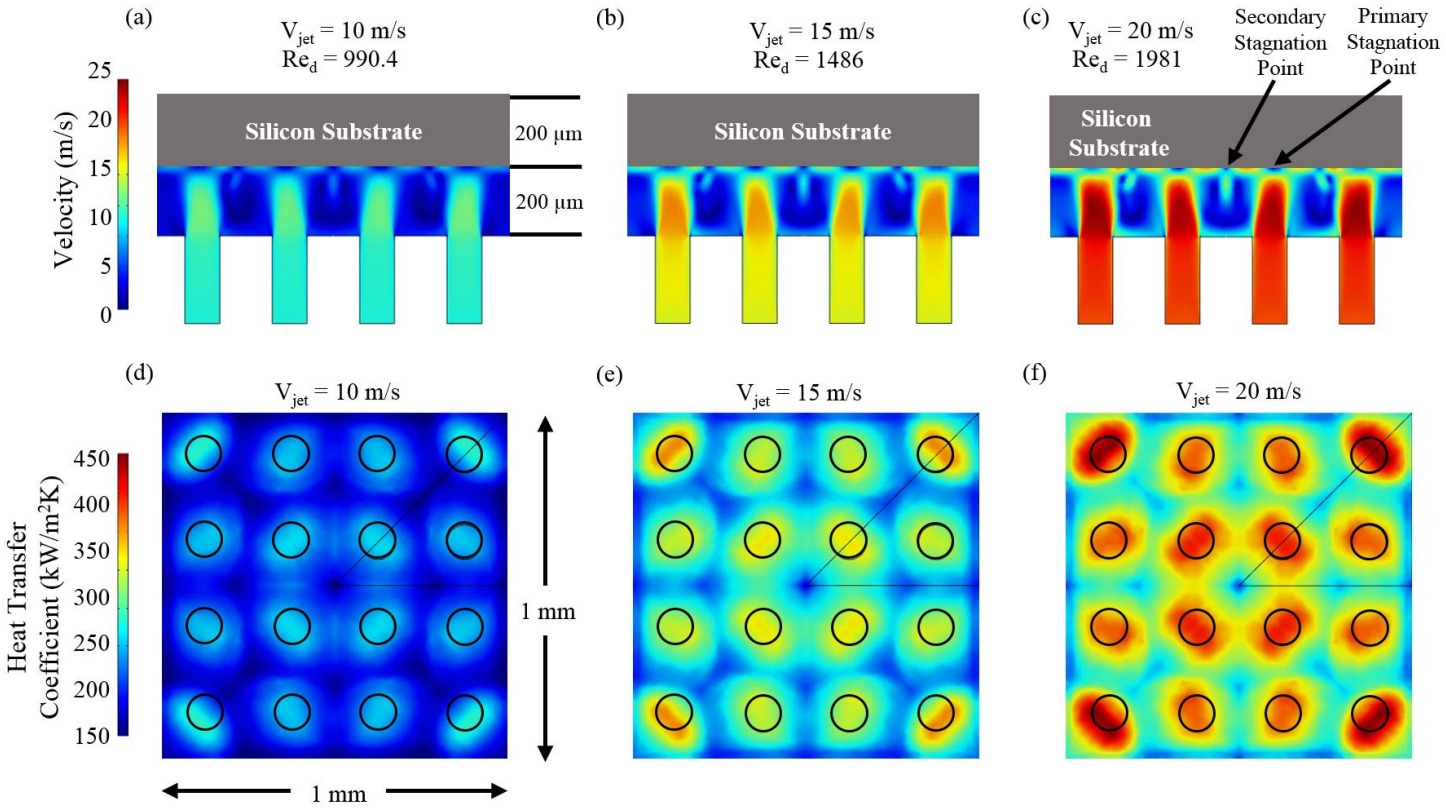

Figure 3: Fluid velocity magnitudes within the microjet cavity at (a) 10 (b) 15, and (c) 20 m/s. Also highlighted in (c) are the primary and secondary stagnation points. Figures (d), (d), and (f) show the heat transfer coefficient at these same velocities. Overlaid are the locations of the microjet orifices. The fluid is water.

The numerical model was used to calculate the heat transfer coefficient by applying a heat flux of 3.75 kW/cm^2 to the top of the silicon substrate. This heat flux is representative of heat fluxes present in high power-density devices, such as gallium nitride (GaN) high electron mobility transistors (HEMTs). The results of the simulation were post processed to compute the local heat transfer coefficients occurring in the 1 mm x 1mm impingement zone on the backside of the silicon substrate. The heat transfer coefficient maps for inlet jet velocities of 10, 15, and 20 m/s are shown in Figs. 3d-3f. The jet geometry showing the location of the 16 jet orifices is overlaid on the map.

As previously discussed, the maximum heat transfer coefficients occur at the stagnation point, the direct centerline of the microjets. In this region, the thermal boundary layer is very thin due to the impact from the jet. The three jet velocities show an increase in both peak and average heat transfer coefficient at the higher jet velocities. Peak heat transfer coefficients of over 400 kW/m^{2}K are predicted and average heat transfer coefficient for the 1 mm x 1 mm heated area for the four velocities shown are 205, 272, and 323 kW/m^{2}K. An additional observation from the heat transfer coefficient maps is the effect of cross flow, where the local maxima are pushed radially outward due to effluent of the other jets. This cross flow effect can be minimized with additional optimization of jet-to-jet spacing, jet-to-target standoff distance, and appropriate routing of effluent.

The heat transfer coefficients are shown for jet velocities ranging from 0.5 to 35 m/s in Fig. 4.

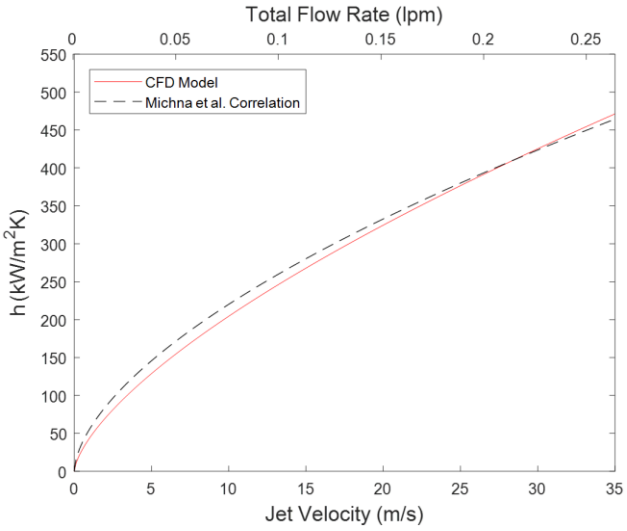

Figure 4: Plot of the average heat transfer coefficient versus the jet velocity with both modeling results from this study and the experimental correlation from Michna et al. for a similar microjet geometry

The average heat transfer coefficients were compared to the experimental correlation developed by Michna et al. in Fig. 4. This correlation was selected due to the similarity in geometry between the devices studied. The Michna et al. Nusselt number

correlation was rearranged to calculate the heat transfer coefficient with the following equation

$$h=\frac{D}{k}0.675Re_d^{0.55}Pr^{0.243}\cos(5.416A_r\text{-}1.259) \quad (5)$$

where the thermo-fluid properties were evaluated at the film temperature. This correlation was used to calculate the area average heat transfer coefficient, which was then compared to the average heat transfer coefficient calculated from the numerical model in this study. The heat transfer coefficient was predicted from the numerical model for the same range of Reynolds numbers studied by Michna et al.

The strong agreement between the numerical model's predicted heat transfer coefficient and the experimental correlation, over the entire range of jet velocities, builds confidence in the accuracy of the model. An exponential fit of the data showed that heat transfer performance scaled with $V^{0.67}$ and thus doubling the flow rate results in improving the heat transfer performance by 1.6x. The increase in performance is achieved with higher jet velocities, at the expense of higher system flow rates and pressure drops.

To further investigate the tradeoff between heat transfer performance and pressure drop, the pressure drop was measured as a function of flow rate. In this experiment, the total flow rate was controlled by the needle valve and measured by the Coriolis flow meter. The pressure drop was measured as the difference between the inlet and outlet pressure transducers. In the plot of Fig. 5, the total flow rate is shown on the upper x-axis. The jet velocity (shown on the bottom x-axis) was calculated by dividing the flow rate by the total cross sectional area of the microjet array. A curve fit of the experimental data showed a second order dependence of pressure drop on jet velocity. With Figures 4 and 5, practitioners can determine, for a needed heat transfer coefficient, what pressure drop and flow rates are appropriate for a microjet system of similar geometric parameters.

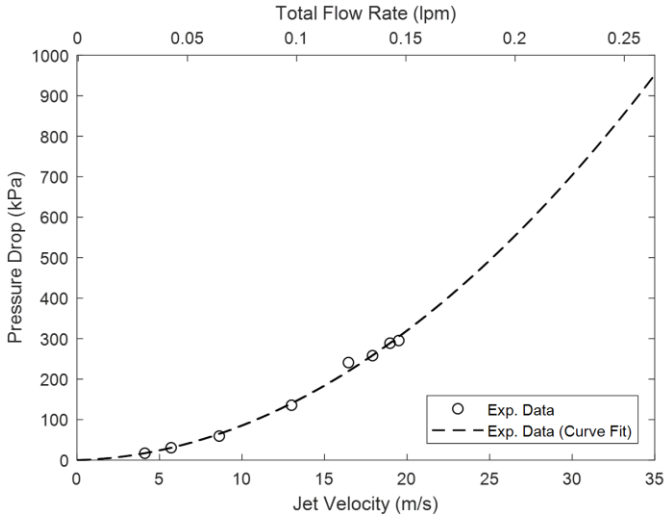

Figure 5: Experimental pressure drop at varying jet velocities (bottom x-axis) and total flow rates (top y-axis)

A second metric of hydraulic performance is the ideal pumping power requirement, Q_{pump}, often expressed with the unit Watts. The ideal pumping power is related to the pressure drop across the jet orifice plate and the total volumetric flow rate in the loop, $\dot{V}$, calculated with

$$Q_{pump}=\Delta P\dot{V} \quad (6)$$

A plot of the ideal pumping power versus average heat transfer coefficient is shown in Fig. 6.

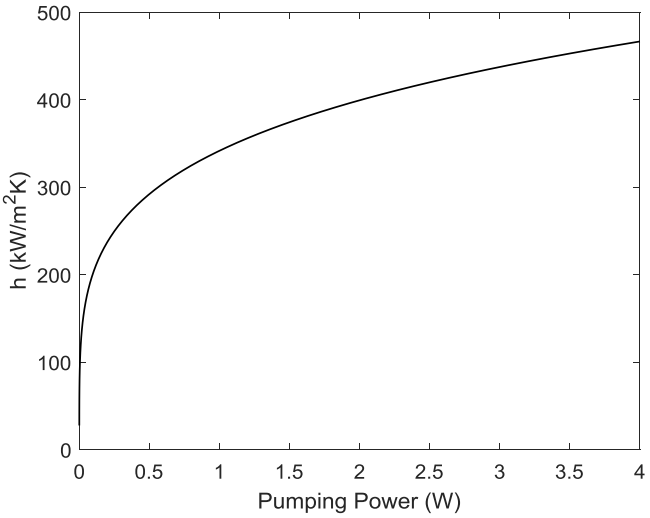

Figure 6: Plot of the required pumping power to achieve the specified heat transfer coefficients

The magnitude of the pumping power to achieve certain heat transfer performance is of interest for meeting certain electronic packaging constraints such as volume requirements or energy consumption. A power fit of the data showed that heat transfer performance scaled with $Q_{pump}^{0.23}$, which indicates a diminishing return at higher pumping powers. For example, getting a 1.6x increase in heat transfer coefficient requires 8x the pumping power. An understanding of this relationship is useful for determining the minimal pumping power required to achieve a certain level of heat transfer performance.

Microjet Clogging

As demonstrated, microjets offer extremely high heat transfer performance at relatively low pumping powers. They achieve such high levels of performance due to momentum and energy exchanges that occur when the high velocity jet interacts with the wall. The performance dependence on velocity raises two practical concerns when considering implementing microjets: clogging and erosion. Clogging of a microjet, either partially or fully, would raise jet velocity in the unclogged jets (but reduce the overall flow rate), as the cross sectional area decreases. The concern for erosion exists because of the momentum exchange that occurs in the impingement zone. To examine the viability of microjet impingement as a long-term electronics cooling solution, a 1000-hour test was performed. This test was meant to simulate operating conditions for an extended period, with the 1000-hour threshold chosen as a

common level for demonstrating lifetime workmanship. In this test, the microjet heater was secured in the fixture and the recirculating chiller was operated for 1000 hours. The flow rate and pressure drop across the orifice were monitored throughout the experiment and are plotted in Fig. 7.

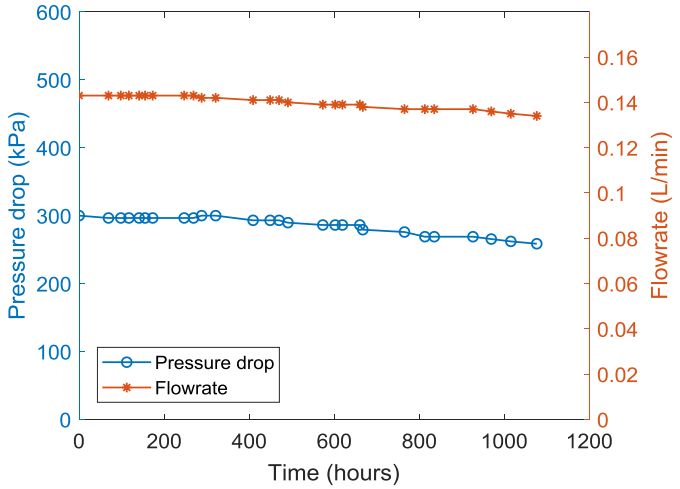

Figure 7: Pressure drop and flow rate recorded during the 1000-hour of continuous microjet impingement

The flow rate and pressure drop remained relatively constant throughout the 1000-hours. The flow rate remained within 6% of its initial value and the pressure drop remained with 12%. The reason for the decrease in flow rate is the accumulation of contaminants in the filter, which was used to remove particles greater than 10 µm from the flow loop. When the filter was replaced after the end of the test, the pressure drop and flow rate were fully restored to their initial values. The 10 µm filter (SS-6TF-10, Swagelok) was relatively inexpensive, ~$10, and can be replaced easily. The filter could also be replaced with a larger particle size filter of 15-20 µm pore size to decrease replacement frequency with minimal effect on clogging.

While no microjet clogging was observed in the monitoring of the pressure drop and flow rate during the 1000-hour test, the possible effects of clogging are highlighted in Fig. 8, where the pressure drop would increase at a particular flow rate due to the clogging of varying percentages of the microjet array. The reason for the increase in pressure drop is that the cross sectional area would decrease, increasing the effective jet velocity at each of the orifices.

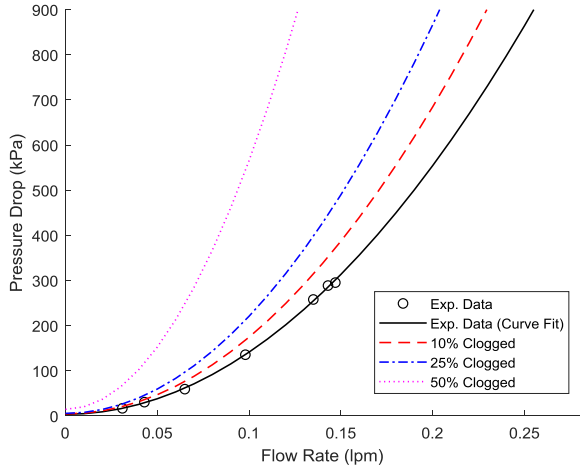

Figure 8: Plot of the pressure drop across the microjet array at varying flow rates. Additional curves show the predicted flow rate for clogging of the 100 µm diameter microjets

An example of the clogging implication would be if two of the microjets were clogged with debris that completely blocked flow, then the pressure drop at a given flow rate would increase by 30-70 kPa through the range of targeted flow rates. As seen in Fig. 9, the pressure drop and flow rate did not experience sudden changes that would be expected with one of the microjet orifices becoming clogged. Additionally, microscope images of the jet orifices at 10x (before and after the 1000-hour test) are shown below in Fig. 9, where there are no discernable indications that one or multiple of the microjets clogged during the testing.

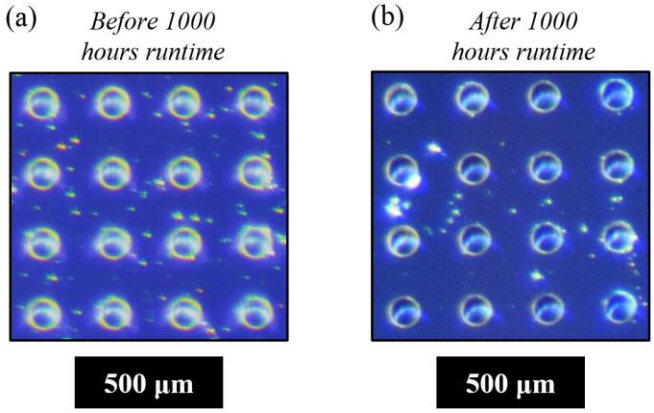

Figure 9: (a) The microjet array before the 1000-hour test (b) The microjet array after the 1000-hour test with no indications of clogging

The takeaway from his portion of the study was that proper filter selection can effectively mitigate the risk of clogging in microjet systems. Such filters can be compact in size, inexpensive, and easily replaceable. This study suggests proper clogging mitigation with filters of pore size less than D/10.

Erosion Inspection

Flow-induced erosion is often cited as a concern with employing microjets due to the impact with the backside of the electronics at relatively high jet velocities. The repeated impacts

of contaminant particles can erode the device and cause anomalous behavior, or, in severe cases, eventual leakage of fluid out of the device. Throughout the 1000-hour test, the area immediately around the microjet assembly was monitored for signs of leaking. The area remained dry the entire 6 weeks, indicating that no catastrophic failures occurred such as the device rupturing. To examine whether there were more subtle indications of erosion, at the conclusion of the test, the microjet array and integrated heater were diced through their centerline as shown in the SEM image in Fig. 10.

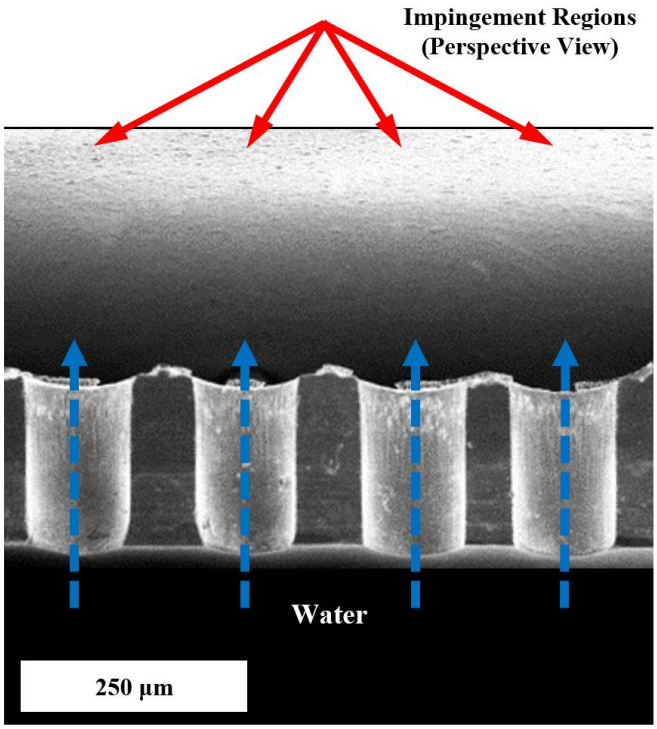

Figure 10: SEM image of the diced microjet assembly after the conclusion of the 1000-hr test, showing no signs of erosion on the backside of the heat generating electronics

The SEM image shows the jet orifices and the backside of the integrated heater with a perspective view. The area with the highest potential for erosion is directly opposite the jets' centerlines, where any particles in the fluid would come in contact with the wall. If there were erosion due to particle blasting, then it would occur in a pattern similar to the microjet array. The SEM image shows a constant surface profile at the backside of the heater, without any indentations opposite the microjets. This shows that the surface of the silicon heater was robust to the continual impact of the high pressure and high velocity jets of water, with possible particle sizes up to 10 µm.

CONCLUSIONS

Jet impingement cooling has been studied for several decades for use in high heat flux applications due to the high heat transfer coefficients. It has recently been identified as a high performance, low SWaP solution for electronics cooling. In this work, we have developed a fully conjugate heat transfer and CFD model of microjet impingement through an array of sixteen 100 µm diameter jet orifices. The model was used to understand the heat transfer interaction occurring at the fluid-surface boundary and predict heat transfer performance at various flow rates, compared to recent empirical correlations.

An experimental setup was constructed, with samples fabricated in silicon, to measure the pressure drop across the microjet plate at various flow rates. The experimental pressure drop measurements and predicted heat transfer performance were used to show the necessary pumping power required to achieve high heat transfer performance. The microjet assembly was tested in a 1000-hour test at high flow rates, showing no signs of clogging or erosion of the backside of the electronic device. The data from this study may be used to estimate the necessary pressure drop and microjet flow rate required to achieve a desired heat transfer coefficient in similar microjet thermal management systems.

NOMENCLATURE

A	Surface area of the heater (m^2)
A_r	Area ratio: jetted area over heated area
CFD	Computational fluid dynamics
D	Jet orifice diameter (m)
GaN	Gallium Nitride
h	Heat transfer coefficient (W/m^2K)
HEMT	High electron mobility transistor
k	Thermal conductivity (W/m-K)
Nu_d	Nusselt number
PEEK	Polyether ether ketone
Pr	Prandtl number
q	Power or heat flux across the device (W)
Q_{pump}	Pumping power required (W)
RANS	Reynolds Averaged Navier Stokes
Re_d	Reynolds number
SEM	Scanning electron microscope
SWaP	Size, Weight and Power
T_f	Fluid inlet temperature (°C)
T_{MP}	Melting point temperature (°C)
T_s	Impact point surface temperature (°C)
V	Jet velocity (m/s)
$\dot{V}$	Total volumetric flow rate (lpm)

Greek Symbols

ΔP	Pressure drop (kPa)
ρ	Density (kg/m^3)
µ	Dynamic viscosity (kg/m-s)

ACKNOWLEDGMENTS

The authors would like to thank Ms. Donna Yost and the MIT Lincoln Laboratory Microelectronics Laboratory for fabricating the heater devices and jet plates. The microjets program was supported by the MIT Lincoln Laboratory RF Systems Line, led by Dr. Jeffrey Herd and Dr. Sean Duffy.

REFERENCES

[1] Incropera, Frank. *Liquid Cooling of Electronic Devices by Single-Phase Convection*. John Wiley and Sons, New York (1999).

[2] Ndao, Sidy, Peles, Yoav, and Jensen, Michael. "Multi-objective thermal design optimization and comparative analysis of electronics cooling technologies." *International Journal of Heat and Mass Transfer* Vol. 52 (2009): pp. 4317-4326.

[3] Walsh, Stephen, Malouin, Bernard, Browne, Eric, Bagnall, Kevin, Wang, Evelyn, and Smith, James. "Embedded Microjets for Thermal Management of High Power-Density Electronic Devices." *(In Review)*

[4] Kandlikar, Satish, Colin, Stephane, Peles, Yoav, Garimella, Srinivas, Pease, Fabian, Brandner, Juergen, and Tuckerman, David. "Heat transfer in microchannels- 2012 status and research needs." *Journal of Heat Transfer* Vo. 135 (2013) p. 091001.

[5] Muszynski, Tomasz and Andrzejczyk, Rafal. "Heat transfer characteristics of hybrid microjet-microchannel cooling module." *Applied Thermal Engineering* Vol. 93 (2016) pp. 1360-1366.

[6] Sung, Myung and Mudawar, Issam. "Single-Phase and Two-Phase Hybrid Cooling Scheme for High-Heat-Flux Thermal Management of Defense Electronics," *Journal of Electronic Packaging* Vol. 131 (2009): p. 021013.

[7] Fabbri, Matteo and Dhir, Vijay. "Optimized Heat Transfer for High Power Electronic Cooling Using Arrays of Microjets," *Journal of Heat Transfer* Vol. 127, No. 7 (2004): pp. 760–769.

[8] Overholt, Matthew, McCandless, Andrew, Kelly, Kevin, Becnel, Charles, and Motakef, Shariar. "Micro-Jet Arrays for Cooling of Electronic Equipment," *Proceedings of the Third International Conference on Microchannels and Minichannels*. ICMM2005-75250: pp. 249–252. Toronto, ON, Canada, June 13-15, 2005.

[9] Browne, Eric, Michna, Gregory, Peles, Yoav, and Jensen, Michael. "Experimental Investigation of Single-Phase Microjet Array Heat Transfer," *Journal of Heat Transfer* Vol. 132 (2010): p. 041013.

[10] Michna, Gregory, Browne, Eric, Peles, Yoav, and Jensen, Michael. "The effect of area ratio on microjet array heat transfer." *International Journal of Heat and Mass Transfer* Vol. 54 (2011): pp. 1782-1790.

[11] Ditri, John, Hahn, Joseph, Cadotte, Roland, McNulty, Michael, and Luppa, Denise. "Embedded cooling of high heat flux electronics utilizing distributed microfluidic impingement jets." *Proceedings ASME International Technical Conference and Exhibition on Packaging and Integration of Electronic and Photonic Microsystems (InterPACK)*, pp. 1-10. San Francisco, CA, USA, July 6-9 2015.

